PCCP

Accepted Manuscript

ROYAL SOCIETY OF CHEMISTRY

www.rsc.org/pccp

Cite this: DOI: 10.1039/c0xx00000x

www.rsc.org/xxxxxx

ARTICLE TYPE

Vibrational Spectroscopy and Theory of $Fe_2^+(CH_4)_n$ (n = 1-3)

Muhammad Affawn Ashraf,[a] Christopher W. Copeland,[a] Abdulkadir Kocak,[a,b] Alexandra R. McEnroe[a] and Ricardo B. Metz[a]*

Received (in XXX, XXX) Xth XXXXXXXXX 20XX, Accepted Xth XXXXXXXXX 20XX

DOI: 10.1039/b000000x

Vibrational spectra are measured for $Fe_2^+(CH_4)_n$ (n = 1-3) in the C-H stretching region (2650-3100 cm^{-1}) using photofragment spectroscopy, by monitoring the loss of CH_4. All of the spectra exhibit an intense peak corresponding to the symmetric C-H stretch around 2800 cm^{-1}. The presence of a single peak suggests a nearly equivalent interaction between the iron dimer and the methane ligands. The peak becomes slightly blue shifted as the number of methane ligands increases. Density functional theory calculations, B3LYP and BPW91, are used to identify possible structures and predict the spectra. Results suggest that the methane(s) bind in a terminal configuration and the complexes are in the octet spin state.

Introduction

Catalytic activation of methane by transition metals is of immense industrial importance, as it would allow broader utilization of an abundant feedstock, and is of fundamental interest because it involves the reaction of the simplest C-H bond. Several third row transition metal atomic cations react with methane under thermal conditions, producing $MCH_2^+ + H_2$.[1,2] Gas phase studies can elucidate the mechanism of C-H activation reactions, since the ions are not affected by the presence of solvent molecules.[3–7] A broader range of methane activation reactions have been observed with metal clusters. For example, although Rh^+ and Au^+ do not activate methane at room temperature,[2,8] Bondybey and coworkers[9] observed methane activation on $Rh_x^+Ar_m$ and Lang *et al.*[10,11] have shown ligand dependent activation of methane on Au_2^+. Additionally, methane activation by Pt^+ and Pt_x^+ shows very specific size dependent reactivity, leading Kummerlöwe *et al.* to suggest that *"the strong reactivity fluctuations over a wide size range are the gas phase fingerprint of a good heterogeneous catalyst material"*.[12] In this vein, Armentrout and coworkers have observed that Fe_x^+ clusters show interesting size dependent reaction thresholds for dehydrogenation of methane, with Fe_4^+ being particularly reactive.[13]

The initial interaction between M_x^+ and methane results in formation of the $M_x^+(CH_4)$ entrance channel complex. This leads to weakening of the C-H bond, which is a prerequisite for C-H activation. A strong interaction between metal and methane(s) leads to a substantial red-shift in the lowest C-H stretching frequencies, and increases their intensity. Measuring this interaction has prompted studies of the vibrational spectroscopy of several $M^+(CH_4)_n$[14–19] and of $Pt_x^+(CH_4)Ar_2$.[20] Our group has studied $Fe^+(CH_4)_n$ (n = 1-4) complexes.[17] As the first step in studies of clusters, here we extend the work to the iron dimer, presenting the vibrational spectra for $Fe_2^+(CH_4)_n$ (n = 1-3). Vibrational spectra of these molecules will answer questions such as the geometry and coordination of the entrance channel complex, and whether the methanes are bound in a terminal fashion or in a bridged configuration. In addition, the spectroscopic fingerprint may also help to identify the spin state of the complex, and whether this changes with the addition of methanes.

Experimental and Computational Methods

Iron dimer ion-methane complexes are produced in a laser ablation source and studied with a dual time-of-flight reflectron mass spectrometer, which has been previously described in detail.[21,22] Iron dimer cations are produced by laser ablation of an iron rod (Sigma-Aldrich, 99.8% pure). The dimer-methane clusters are generated in an expansion gas mixture of 5-10% methane in helium at 60-120 psi backing pressure. Ions produced then expand supersonically into vacuum and cool to a rotational temperature of ~10K.[23] Ions are then skimmed into a differentially pumped chamber and enter the extraction region of a Wiley-McLaren time-of-flight mass spectrometer.[24] Ions are accelerated to 1800 V of kinetic energy, then re-referenced to ground before entering the field free flight tube. Mass selected ions are photodissociated at the turning point of the reflectron using an IR laser system. Parent and photofragment ions re-accelerate out of the reflectron, traverse a field-free region, and impinge upon a 40 mm diameter dual microchannel plate detector. Masses are determined from their characteristic flight times. The infrared (IR) laser system is an Nd:YAG pumped optical parametric oscillator/optical parametric amplifier that is tunable from 2 to 4.5 μm, producing a ~6 mJ pulse near 3100 cm^{-1}. In the reflectron region a multipass setup for the IR beam is installed which lets it traverse the ion beam ~15 times.[25] The laser wavelength is calibrated using CH_4 absorptions.

The ion signal is amplified, collected on a digital oscilloscope or gated integrator, and averaged with a LabView based program. The photodissociation spectrum is obtained by monitoring the

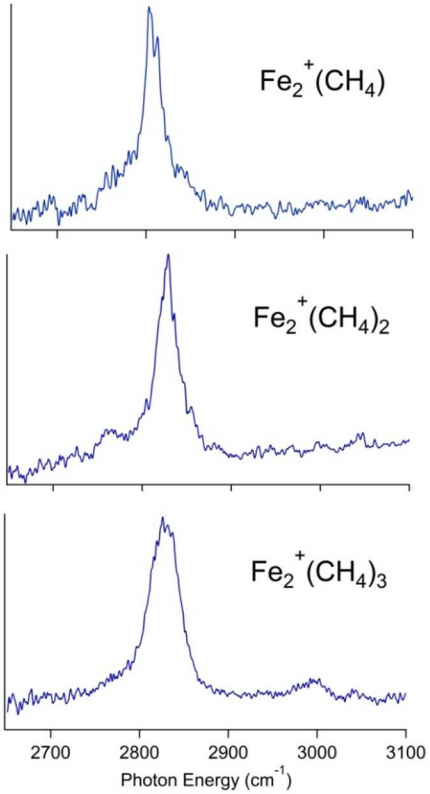

Figure 1. Infrared photodissociation spectra of $Fe_2^+(CH_4)_n$ (n = 1-3) in the C-H stretching region.

Species	$2S+1$	Relative Energy (kJ/mol)	Bond Dissociation Energy (cm^{-1})
Fe_2^+	8	0.0 (0.0)	--
	6	118.0 (98.5)	--
$Fe_2^+(CH_4)$	8	0.0 (0.0)	3304 (3344)
	6	113.7 (85.4)	3659 (4437)
$Fe_2^+(CH_4)_2$	8	0.0 (0.0)	1843 (1931)
	6	94.7 (55.5)	3428 (4435)
$Fe_2^+(CH_4)_3$	8	0.0 (0.0)	809 (1566)
	6	64.6 (11.4)	3327 (5255)

Table 1. Relative energies and spin-allowed $Fe_2^+(CH_4)_{n-1}$-(CH_4) dissociation energies calculated with the B3LYP and BPW91 (parentheses) functionals and 6-311++G(3df,3pd) basis.

yield of the fragment ion of interest as a function of wavelength and normalizing to parent ion signal and laser fluence. The photodissociation spectrum is the product of the absorption and the photodissociation quantum yield. The photodissociation yield is calculated by dividing the fragment ion signal when the IR laser is on, by the parent ion signal when the IR laser is off. It varies from 9% to 30% depending upon the ion.

Computations are carried out using the Gaussian 09 program package.[26] Optimized geometries of the ions are calculated using the Becke Lee-Yang-Parr hybrid HF/DFT (B3LYP) and BPW91/DFT method and the 6-311++G(3df,3pd) basis set.

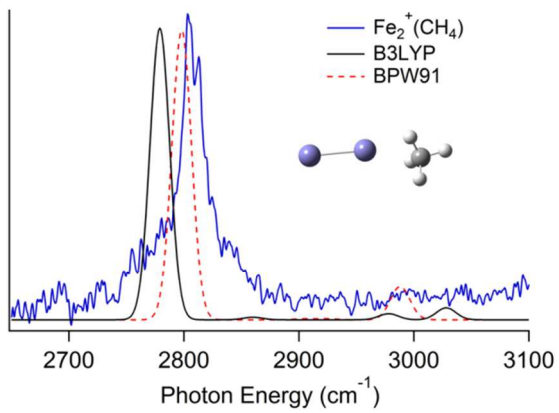

Figure 2. Experimental IR photodissociation spectrum of $Fe_2^+(CH_4)$ along with the simulated spectra using the B3LYP and BPW91 functionals. The structure is the octet state of the molecule according to B3LYP.

The calculated vibrational frequencies are harmonic, whereas the measured vibrational frequencies include anharmonicity. To include this effect, the calculated frequencies are scaled by the ratio of the experimental and calculated C-H stretching frequencies of isolated CH_4 (ν_1 = 2917 cm^{-1}, ν_3 = 3019 cm^{-1}) which is 0.963 for B3LYP and 0.979 for BPW91. Calculated spectra are convoluted with a 20 cm^{-1} fwhm Gaussian for comparison with experiment. All reported energies include zero-point energy.

Results

Vibrational spectra of $Fe_2^+(CH_4)_n$ (n = 1 - 3). Vibrational spectra measured using photofragment spectroscopy are presented in figure 1. The spectra show a single peak between 2800 cm^{-1} and 2830 cm^{-1} for all the species. This corresponds to a red shift of ~100 cm^{-1} in the symmetric stretch of bare CH_4. The peak becomes less red shifted as the number of methanes on the cluster increases. Since all the spectra show peaks at similar positions, we infer that the clusters exhibit similar geometries. To determine the structure and characterize the vibrations of each $Fe_2^+(CH_4)_n$ cluster, we carry out geometry optimization and vibrational frequency calculations for several potential isomers and spin states. Our previous studies of metal ion-methane complexes $[M^+(CH_4)_n]$ have shown that the B3LYP hybrid density functional does a good job in predicting the observed vibrational spectra.[17–19] On the other hand, a detailed comparison of several DFT methods on neutral and charged iron clusters $Fe_x^{0/+/-}$ showed that the non-hybrid BPW91 functional is preferable over B3LYP.[27,28] It is thus somewhat of an open question as to which functional is most appropriate for metal cluster ion-ligand complexes such as $Fe_2^+(CH_4)_n$.

Although the ground state of Fe_2^+ has not been determined experimentally, it has been the subject of many computational studies. Recent multireference calculations (RASPT2) by Hoyer *et al.*[29] predict a $^8\Sigma_u^-$ ground state, with a $^8\Delta_u$ state at 44 kJ/mol. The lowest lying dectet state is 129 kJ/mol above the ground state. Benchmark calculations at this level are not practical for larger clusters containing significantly more metal atoms or multiple or complex ligands, hence the need for DFT

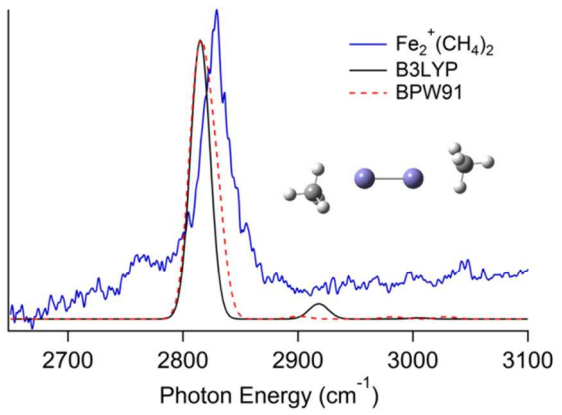

Figure 3. Experimental IR photodissociation spectrum of $Fe_2^+(CH_4)_2$ along with the simulated B3LYP and BPW91 spectra. The structure is the octet state of the molecule according to B3LYP.

calculations. Table 1 summarizes computational results with the B3LYP and BPW91 functionals. The calculations predict the ground state of Fe_2^+ is $^8\Delta_u$ consistent with previous BPW91 results.[27,30] Our calculations predict both the sextet and dectet are significantly higher in energy than the octet state. Chiodo *et al.* predict a $^{10}\Sigma_u^+$ ground state, 7 kJ/mol below the $^8\Sigma_u$ at the B3LYP/$DZVP_{opt}$ level. The present B3LYP study, using the larger 6-311++G(3df,3pd) basis set, predicts the dectet state lies 74 kJ/mol above the octet ground state. All of the $Fe_2^+(CH_4)_n$ clusters with n=1-3, are predicted to have an octet ground state; the dectet states are calculated to be at least 100 kJ/mol higher in energy. However, as the number of ligands increases, the energy difference between the sextet and the octet states progressively decreases. The sextet states generally have valence electron occupancy $3d^{14}4s^1$, resulting in a stronger interaction with ligands than the octet state ($3d^{13}4s^2$); the dectet states ($3d^{12}4s^3$) interact with ligands even more weakly.[29,30]

Discussion

$Fe_2^+(CH_4)$. The spectrum of $Fe_2^+(CH_4)$ (figure 2) shows a single intense peak at 2803 cm^{-1} with 26 cm^{-1} fwhm. The photodissociation yield is 9%. Similar photodissociation yields are observed for $M^+(CH_4)Ar_2$ (M = Co, Ni, Cu), which have similar calculated C-H absorption intensity for the lowest C-H stretch and where the low Ar binding energy ensures that one photon has sufficient energy to dissociate the complex.[18,19] This suggests that photodissociation of $Fe_2^+(CH_4)$ also has a quantum yield of one and is a single photon process at ~2800 cm^{-1}, suggesting that the calculations slightly overestimate the methane binding energy.

The B3LYP and BPW91 functionals predict similar geometries for $Fe_2^+(CH_4)$. The hydrogen atoms have connectivity of nearly η^3, slightly distorted towards η^2, leading to overall C_s symmetry. The Fe-C distance is calculated to be 2.389 Å (B3LYP), and 2.300 Å (BPW91). Geometry optimizations starting from several η^2 structures and bridged structures all relax to the η^3 ground state. Detailed geometries, energies and vibrational frequencies for all species are given in Table S1. The calculated binding energies and geometries are similar to those obtained by Chiodo *et al.* in their study of the reaction of Fe_2^+ with methane.[30] They predict the Fe_2^+-CH_4 binding energy to be 3850 cm^{-1} and 3532 cm^{-1} at the B3LYP/$DZVP_{opt}$ and BPW91/$DZVP_{opt}$ level of theory respectively.[30] These binding energies are slightly higher than those obtained using the 6-311++G(3df, 3pd) basis set; both basis sets predict η^3 hydrogen coordination and very similar Fe-C bond distances.

The BPW91 calculation predicts a strong peak at 2798 cm^{-1}; the remaining C-H stretch absorptions are very weak. Thus, the simulated spectrum matches the experiment very well. The B3LYP calculated spectrum is similar, with a peak at 2779 cm^{-1}, about 20 cm^{-1} below the observed peak. The observed 2803 cm^{-1} vibration corresponds to the symmetric C-H stretch, with all C-H bonds stretching in phase, with substantially larger amplitude for the three proximate C-H bonds than the distal.

$Fe_2^+(CH_4)_2$. The spectrum of $Fe_2^+(CH_4)_2$ (figure 3) shows a single intense peak at 2829 cm^{-1} with 25 cm^{-1} fwhm. The photodissociation yield for $Fe_2^+(CH_4)_2$ is observed to be 30% suggesting single photon photodissociation. The calculated absorption intensity for this vibration is twice that of the corresponding vibration in $Fe_2^+(CH_4)$, leading to the increased photodissociation yield. The calculated binding energies of ~1900 cm^{-1} are consistent with single photon dissociation.

The B3LYP calculation predicts two stable structures that can contribute to the spectrum. The ground state has each iron coordinated to one CH_4. In this structure, both the CH_4 are equivalent, with a 2.462 Å Fe-C bond. As a result, the predicted spectrum has a single peak at 2814 cm^{-1}, as shown in figure 3. The calculations predict hydrogen atom connectivity of nearly η^3, slightly distorted towards η^2. There is a second local minimum, ~380 cm^{-1} higher in energy, in which both ligands are bound to one of the iron atoms. The resulting spectrum is calculated to have a doublet at 2803/2833 cm^{-1}, as shown in table S2A. As the observed spectrum consists of a single peak, this structure is at most a minor contributor to the experiment. Similar to $Fe_2^+(CH_4)$, structures with bridging methanes relax to the ground state terminal structure. Simulated spectra of structures in which each iron is coordinated to one methane are in good accord with the experimental spectrum and reproduce the experimental observation that the addition of the second CH_4 leads to a reduced red shift in the spectrum.

The BPW91 calculation predicts similar structures. In the isomer with each Fe interacting with one CH_4, the Fe-C distances are 2.405 Å and 2.512 Å. As a result of the non-equivalent Fe-C interactions, the vibrational spectrum has a peak at 2814 cm^{-1} with a shoulder at 2827 cm^{-1}. This leads to a broader peak centered at 2816 cm^{-1}, as shown in figure 3. The other isomer, in which both CH_4 are bound to one iron, is calculated to be the ground state, 635 cm^{-1} lower in energy. However, the predicted spectrum (table S2B) is red shifted by 200 cm^{-1}, clearly not in accord with the experiment.

$Fe_2^+(CH_4)_3$ The spectrum of $Fe_2^+(CH_4)_3$ (figure 4) shows a peak centered at 2830 cm^{-1}. The peak is significantly broader than those of the smaller clusters, with 36 cm^{-1} fwhm. The spectrum

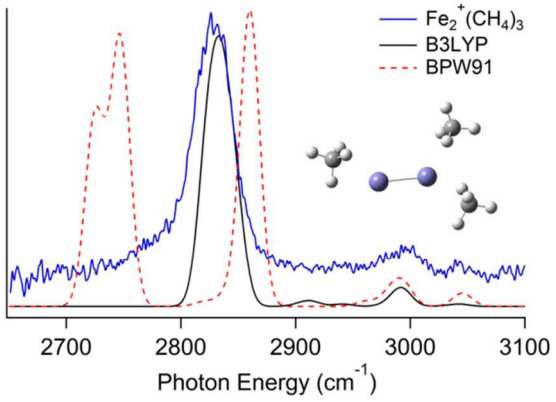

Figure 4. Experimental IR photodissociation spectrum of $Fe_2^+(CH_4)_3$ along with the simulated B3LYP and BPW91 spectra. The B3LYP structure is shown.

also shows a much smaller peak centered at 3000 cm^{-1}. The BPW91 calculation predicts that the three CH_4 are clearly not equivalent. One of the iron atoms interacts strongly with two CH_4, resulting in Fe-C bond distances of 2.368 Å and 2.419 Å respectively, with hydrogen atom connectivity of approximately η^2. The other iron interacts weakly with the CH_4 proximal to it, at a bond distance of 2.640 Å and it has η^3 coordination. As a result of such a non-degenerate interaction, the predicted spectrum has three intense peaks at 2725, 2747, and 2860 cm^{-1}. The resulting simulated spectrum clearly disagrees with the observed spectrum. In contrast, the B3LYP calculation predicts the interaction of the three methanes to be very similar. Two of the CH_4 interact with one of the irons with Fe-C bond distances of 2.509 Å (η^2/η^3 coordination) and 2.671 Å (η^2 coordination) respectively, while the third CH_4 interacts with the proximal iron at a bond distance of 2.527 Å, and it has η^3 hydrogen coordination. As a result, the B3LYP calculation predicts three very closely lying peaks at 2822, 2834 and 2846 cm^{-1}. This leads to a single broad peak centered at 2832 cm^{-1}. The close vicinity of these peaks indicates that the three CH_4 have a similar interaction with the iron dimer. The simulated spectrum predicted by the B3LYP calculation is an excellent match to the experimental spectrum. The simulation also suggests that the breadth of the experimental peak is due to nearly degenerate unresolved C-H stretching vibrations, characteristic of a complex with three nearly equivalent CH_4. Again, geometries with bridging methanes relax to the ground state terminal structure. For $Fe_2^+(CH_4)_3$ the calculations predict that the sextet state does not lie very far above the octet. Because the sextet interacts more strongly with CH_4 than the octet state, it leads to a highly red-shifted spectrum (Table S1), which is not consistent with the experimental spectrum.

Conclusions

In this work, we present vibrational spectra of $Fe_2^+(CH_4)_n$ (n = 1-3) obtained by monitoring the loss of CH_4 following IR photoexcitation. We calculated and compared vibrational spectra using the B3LYP and BPW91 functionals. Both calculations predict the ground state of Fe_2^+ and the ligated clusters to be octets. Comparison of the experimental spectra to simulated spectra for various potential isomers and spin states suggests terminal binding of the methane(s). The observation of a single intense peak for $Fe_2^+(CH_4)$, $Fe_2^+(CH_4)_2$ and $Fe_2^+(CH_4)_3$ suggests that the additional methanes interact in a nearly equivalent manner with the iron dimer. As the number of methanes increases, the position of the peak slightly blue shifts, moving closer to the symmetric C-H stretch at 2917 cm^{-1}, indicating a weakening of the metal-methane interaction.

Our previous studies[17] of $Fe^+(CH_4)_n$ complexes show >100 cm^{-1} larger red shifts than is observed for the metal dimer. This correlates with the higher sequential methane binding energies for the metal atom[31–33] and with guided ion beam studies that find lower threshold for dehydrogenation of methane by Fe^+ than Fe_2^+.[13] Spectroscopic and computational studies of larger $Fe_x^+(CH_4)_n$ (x > 2) clusters are ongoing.

Notes

Financial support from the National Science Foundation under award CHE-1300501 is gratefully acknowledged. Some of the calculations were carried out at the Massachusetts Green High Performance Computing Center.

[a] *Department of Chemistry, University of Massachusetts Amherst, Amherst, Massachusetts 01003 Fax: 413-545-4490; Tel: 413-545-6089; E-mail: rbmetz@chem.umass.edu*
[b] *Current Address: Department of Chemistry, Gebze Teknik Üniversitesi, Gebze, Turkey.*

† Electronic Supplementary Information (ESI) available: [Table S1: Energies and geometries of $Fe_2^+(CH_4)_n$ (n = 1-3), octet and sextet states, at the B3LYP/6-311++G(3df,3pd) and BPW91/6-311++G(3df,3pd) level, Table S2: Energies and geometries of $Fe_2^+(CH_4)_2$ where both CH_4 are attached to a single iron]. See DOI: 10.1039/b000000x/

References

1 K. K. Irikura and J. L. Beauchamp, *J. Phys. Chem.*, 1991, **95**, 8344–8351.

2 A. Shayesteh, V. V. Lavrov, G. K. Koyanagi and D. K. Bohme, *J. Phys. Chem. A*, 2009, **113**, 5602–5611.

3 H. Schwarz, *Angew. Chemie - Int. Ed.*, 2011, **50**, 10096–10115.

4 H. Schwarz, *Isr. J. Chem.*, 2014, **54**, 1413–1431.

5 J. Roithova and D. Schröder, *Chem. Rev.*, 2010, **110**, 1170–1211.

6 J. Roithová, *Chem. Soc. Rev.*, 2012, **41**, 547.

7 P. B. Armentrout, *Catal. Sci. Technol.*, 2014, **4**, 2741–2755.

8 Y. M. Chen and P. B. Armentrout, *J. Phys. Chem.*, 1995, **99**, 10775–10779.

9 G. Albert, C. Berg, M. Beyer, U. Achatz, S. Joos, G. Niedner-Schatteburg and V. E. Bondybey, *Chem. Phys. Lett.*, 1997, **268**, 235–241.

10 S. M. Lang, T. M. Bernhardt, R. N. Barnett and U. Landman, *Angew. Chemie - Int. Ed.*, 2010, **49**, 980–983.

11 S. M. Lang, T. M. Bernhardt, R. N. Barnett and U. Landman, *J. Phys. Chem. C*, 2011, **115**, 6788–6795.

12 G. Kummerlöwe, I. Balteanu, Z. Sun, O. P. Balaj, V. E. Bondybey and M. K. Beyer, *Int. J. Mass Spectrom.*, 2006, **254**, 183–188.

13 R. Liyanage, X.-G. Zhang and P. B. Armentrout, *J. Chem. Phys.*, 2001, **115**, 9747.

14 O. Rodriguez and J. M. Lisy, *Chem. Phys. Lett.*, 2011, **502**, 145–149.

15 B. L. J. Poad, C. D. Thompson and E. J. Bieske, *Chem. Phys.*, 2008, **346**, 176–181.

16 V. Dryza and E. J. Bieske, *Int. J. Mass Spectrom.*, 2010, **297**, 46–54.

17 M. Citir, G. Altinay, G. Austein-Miller and R. B. Metz, *J. Phys. Chem. A*, 2010, **114**, 11322–11329.

18 A. Kocak, Z. Sallese, M. D. Johnston and R. B. Metz, *J. Phys. Chem. A*, 2014, **118**, 3253–3265.

19 A. Kocak, M. A. Ashraf and R. B. Metz, *to be submitted*, .

20 D. J. Harding, C. Kerpal, G. Meijer and A. Fielicke, *Angew. Chemie - Int. Ed.*, 2012, **51**, 817–819.

21 R. B. Metz, *Int. Rev. Phys. Chem.*, 2004, **23**, 79–108.

22 J. Husband, F. Aguirre, P. Ferguson and R. B. Metz, *J. Chem. Phys.*, 1999, **111**, 1433–1437.

23 F. Aguirre, J. Husband, C. J. Thompson, K. L. Stringer and R. B. Metz, *J. Chem. Phys.*, 2003, **119**, 10194–10201.

24 W. C. Wiley and I. H. McLaren, *Rev. Sci. Instrum.*, 1955, **26**, 1150–1157.

25 G. Altinay and R. B. Metz, *J. Am. Soc. Mass Spectrom.*, 2010, **21**, 750–757.

26 M. J. Frisch, G. W. Trucks, H. B. Schlegel, G. E. Scuseria, M. A. Robb, J. R. Cheeseman, G. Scalmani, V. Barone, B. Mennucci, G. A. Petersson, H. Nakatsuji, M. Caricato, X. Li, H. P. Hratchian, A. F. Izmaylov, J. Bloino, G. Zheng, J. L. Sonnenberg, M. Hada, M. Ehara, K. Toyota, R. Fukuda, J. Hasegawa, M. Ishida, T. Nakajima, Y. Honda, O. Kitao, H. Nakai, T. Vreven, J. A. Montgomery Jr., J. E. Peralta, F. Ogliaro, M. Bearpark, J. J. Heyd, E. Brothers, K. N. Kudin, V. N. Staroverov, T. Keith, R. Kobayashi, J. Normand, K. Raghavachari, A. Rendell, J. C. Burant, S. S. Iyengar, J. Tomasi, M. Cossi, N. Rega, J. M. Millam, M. Klene, J. E. Knox, J. B. Cross, V. Bakken, C. Adamo, J. Jaramillo, R. Gomperts, R. E. Stratmann, O. Yazyev, A. J. Austin, R. Cammi, C. Pomelli, J. W. Ochterski, R. L. Martin, K. Morokuma, V. G. Zakrzewski, G. A. Voth, P. Salvador, J. J. Dannenberg, S. Dapprich, A. D. Daniels, Ö. Farkas, J. B. Foresman, J. V Ortiz, J. Cioslowski and D. J. Fox, *Gaussian 09, Rev. D01, Gaussian Inc.,Wallingford CT*, 2013.

27 G. L. Gutsev and C. W. Bauschlicher, *J. Phys. Chem. A*, 2003, **107**, 7013–7023.

28 G. L. Gutsev, C. a Weatherford, P. Jena, E. Johnson and B. R. Ramachandran, *J. Phys. Chem. A*, 2012, **116**, 10218–28.

29 C. E. Hoyer, G. L. Manni, D. G. Truhlar and L. Gagliardi, *J. Chem. Phys.*, 2014, **141**, 204309.

30 S. Chiodo, I. Rivalta, M. Del Carmen Michelini, N. Russo, E. Sicilia and J. M. Ugalde, *J. Phys. Chem. A*, 2006, **110**, 12501–12511.

31 P. B. Armentrout and B. L. Kickel, in *Organometallic Ion Chemistry*, ed. B. S. Freiser, Kluwer Academic Publishers, Dordrecht, The Netherlands, 1994, p. 1.

32 R. H. Schultz and P. B. Armentrout, *J. Phys. Chem.*, 1993, **97**, 596–603.

33 Q. Zhang, P. R. Kemper and M. T. Bowers, 2001, **211**, 265–281.